CT virtual intravascular endoscopy in the visualization of coronary plaques: A pictorial essay

Zhonghua Sun [1], Lei Xu[2]

1. Department of Medical Radiation Sciences, Curtin University, Perth, Western Australia, 6845, Australia
2. Department of Radiology, Beijing Anzhen Hospital, Capital Medical University, Beijing, China

Corresponding author:

Prof Lei Xu, Department of Radiology, Beijing Anzhen Hospital, Capital Medical University, No. 2, Anzhen Road, Chaoyang District, 100029, Beijing, China

Tel: +86-10-64456071

Fax: +86-10-64456962

Email: leixu2001@hotmail.com

Abstract

Coronary CT angiography has been increasingly used to diagnose coronary artery disease with high diagnostic value achieved. For further assessment of coronary lumen stenosis, coronary CT angiography allows characterization of coronary plaques in terms of plaque morphology and composition. Coronary plaques are commonly assessed on 2D axial and multiplanar reformatted images. However, these visualization tools are limited to viewing extraluminal changes in the coronary artery but fail to provide intraluminal appearances of the coronary wall due to presence of plaques. In this pictorial essay, we present various intraluminal appearances of coronary wall and plaques with use of 3D virtual intravascular endoscopy (VIE) visualization in relation to different types of plaques. VIE appearances of coronary stents in patients treated with coronary stenting are also briefly demonstrated to show both normal stents and in-stent restenosis.

Keywords: Coronary artery disease, coronary CT angiography, plaque, virtual intravascular endoscopy, visualization

Introduction

Coronary CT angiography (CCTA) is a well-established less invasive imaging modality for the diagnosis of coronary artery disease (CAD) with high diagnostic value having been reported in many studies [1-10]. In addition to the detection and assessment of coronary artery stenosis, CCTA allows characterization of coronary plaques in terms of plaque components [11-13]. It is generally agreed that plaque composition rather than the degree of luminal narrowing may provide more accurate information for prediction of the patient's risk for further cardiac events [14]. Specific plaques features such as low-attenuation area, positive remodelling, spotty calcification and napkin ring sign demonstrated by CCTA have been reported to be directly related to the development of major adverse cardiac events [15-19]. Therefore, analysis of plaque features plays an important role in the identification of high-risk patients.

Assessment of coronary plaques is commonly performed with use of 2D axial and multiplanar reformatted as well as 3D volume rendering images. However, the main limitation of these visualizations is lack of direct intraluminal views of plaque appearances and corresponding coronary wall changes. This limitation is overcome by a 3D visualization technique, virtual intravascular endoscopy (VIE) which is proved to have diagnostic applications in cardiovascular disease [20-25]. These previous studies have shown that VIE offers additional value to conventional visualizations for accurate assessment of cardiovascular disease. Accurate assessment of plaque morphology with subsequent coronary wall changes helps identification of high-risk patients by detecting vulnerable plaques, thus leading to better risk stratification and patient management [19, 21, 25]. In this pictorial

essay, we further extend the applications of VIE to coronary artery disease with the aim of demonstrating a spectrum of intravascular appearances of coronary plaques in a group of patients with suspected CAD. Furthermore, VIE visualization of coronary stents is also presented in patients treated with coronary stenting.

Patient data and CCTA scanning protocol

One hundred patients (80 male, mean age 58 years, age range 41-77 years old) with suspected CAD and atherosclerotic plaques on CCTA and another 13 patients (9 male, mean age 62 years, age range 47-71 years old) treated with coronary stents who underwent CCTA examinations were retrospectively reviewed and included in the study. The institutional review board approval was waived in this study since these patients were referred for CCTA scans as a routine procedure for clinical diagnosis. Patients' details were de-identified in all of the images, thus, no informed consent was obtained from these patients.

CCTA of patients with suspected CAD was performed with retrospective ECG-gating on a first generation dual-source (DSCT) CT (Somatom Definition, Siemens Healthcare, Forchheim, Germany) in 30 patients, a second generation DSCT (Somatom Definition Flash; Siemens Healthcare, Forchheim, Germany) in 45 patients and with prospective gating on 320-slice CT (Toshiba Aquilion ONE, Toshiba, Otawara, Japan) in 25 patients; while CCTA was performed on a first generation DSCT (Somatom Definition, Siemens Healthcare, Forchheim, Germany) in 13 patients treated with coronary stenting. The scanning protocols for these CT scanners were as follows: detector collimation 2 x 32 x 0.6 mm, gantry rotation of 0.33 s, with a tube voltage of 100-120 kVp depending on body mass index

(BMI) and tube current ranging from 345 to 420 mAs/rot for the first generation DSCT; detector collimation 2 x 64 x 0.6 mm, gantry rotation of 0.28 s, with a tube voltage of 100-120 kVp depending on BMI and tube current ranging from 330-450 mAs/rot for the second generation DSCT; detector collimation 320 x 0.5 mm, gantry rotation of 0.35 s, with a tube voltage of 100-120 kVp depending on BMI and automatic tube current modulation for the 320-slice CT, respectively. Beta-blockers were administered in patients with heart rate more than 65 bpm (beats per minute) for 320-slice CT scanning and in patients with heart rate more than 80 bpm for DSCT scanning.

Non-ionic contrast medium Iopromide (370 mg/ml, Bayer Schering Pharma) was injected using a dual-head power injector with use of bolus tracking technique with a CT attenuation of 120 Hounsfield Unit (HU) as the triggering threshold in the ascending aorta to initiate the scan. Sixty to 75 ml contrast medium was injected at an injection rate of 4.5-5.5 ml/s in the 120 kV protocol, and 50-65 ml contrast medium at an injection rate of 4-4.5 ml/s in the 100 kV protocol. All injections were followed by 30 ml of saline flush. ECG tube current modulation was used with full tube current from 30% to 75% of the R-R interval. Pitch varied from 0.2-0.4 and depended on the heart rate for DSCT protocols. Images were reconstructed using 0.6-0.75 mm slice thickness and 0.5-0.6 mm increments for DSCT, 0.5 mm and interval of 0.25 mm for 320-slice CT, respectively.

CCTA findings in coronary artery disease and coronary stenting

Coronary plaques were most commonly detected in the left anterior descending (LAD) coronary artery, which was observed in 35% of the cases, followed by 25%, 20% and 10% of cases involving both the LAD and left circumflex (LCx), all of the three main coronary vessels, and the right coronary artery

(RCA), respectively. Plaques involving both the LAD and RCA were found in the remaining 10% of patients.

Of 13 patients treated with coronary stents, CCTA findings were found normal with patent coronary stents in 8 patients, while in-stent restenosis was suspected in the remaining 5 patients. Of 8 patients with patent stents, a total of 11 stents were placed in the coronary arteries with 7 in LAD, 3 in RCA and 1 in LCx, respectively. Of 5 patients with suspected in-stent restenosis, a total of 6 stents were placed in the coronary arteries with 3 in LAD, 2 in LCx and 1in RCA, respectively.

Generation of VIE images

CT volume data were converted from original DICOM (digital imaging and communications in medicine) images which were transferred to a workstation equipped with Analyze V 11.0 (AnalyzeDirect, Inc., Lexana, KS, USA) for generation of 3D VIE images. Post-processing of CT data was performed with a CT number thresholding technique, which was previously described [26-28]. In summary, the first step was to measure the CT attenuation at the main coronary arteries, namely right and left coronary arteries to determine the threshold that was used to remove the contrast-enhanced blood from the coronary artery. Then the CT threshold value which was measured between 200 HU and 350 HU in the first step was applied to generate the intraluminal views of coronary artery ostium, lumen surface and coronary plaques. Once an averaged threshold is determined, the upper threshold is progressively changed, in steps of 20 HU to detect alterations in the coronary wall and plaque surface. This ensures that floating shape and other artifacts are avoided in the final VIE images. Figure 1 shows the relationship between generation of VIE views of left coronary ostium and selection of an

appropriate threshold. The intraluminal appearance of the coronary ostium or plaque could be irregular or distorted due to presence of artifacts if an inappropriate threshold is selected, which could affect visualization and assessment of coronary lesions.

Since coronary artery is relative small in diameter (3-5 mm), thus, intraluminal appearance of the coronary ostium and plaques visualized on VIE images need to be correlated with corresponding orthogonal views to verify the exact anatomic details (Fig 2). This ensures accurate identification of the location of both normal anatomic structures and abnormal wall changes.

VIE appearances of normal coronary artery wall

In normal coronary artery without presence of coronary plaques or atherosclerotic changes, the coronary wall appears smooth with clear demonstration of the coronary ostial configuration and lumen on VIE visualization. Figure 3 is an example showing the normal intraluminal appearance of left coronary ostia corresponding to different branches arising from the left coronary artery, while Figure 4 shows the normal right coronary ostium as shown on VIE visualization.

VIE appearances of coronary plaques

VIE appearances of plaques and consequent coronary wall changes depend on the type, composition and extent of the plaques. Furthermore, the position or location of the plaques in relation to the artery wall can be assessed in terms of eccentric or concentric appearances, whether the coronary ostium is covered by the plaques or spared from coverage. VIE appearances corresponding to different types of plaques are presented in the following sections.

Non-calcified plaques

Non-calcified plaques are commonly shown on VIE as smooth, protruding sign arising from the coronary wall (Fig 5). In order to demonstrate the non-calcified plaque in relation to the surrounding coronary artery ostia, attention should be paid to changing the CT threshold when the viewing position is moved from the normal coronary artery to the location where plaque is located, as CT attenuation of non-calcified plaque is much lower than that of contrast-enhanced blood in the coronary artery. Figure 6 shows a non-calcified plaque at the proximal segment of LAD on multiplanar reformatted image, while corresponding VIE of the plaque can only be seen clearly when the upper CT threshold is lowered from 140 to 60 HU.

Calcified plaques

Calcified plaques are usually shown as a protruding sign with smooth appearance on VIE. The position or location of the plaques in relation to the artery wall can be accurately assessed in terms of eccentric (Figs 7, 8) or concentric appearance (Figs 9, 10), or luminal changes regarding the involvement of superior or inferior portion of the wall (Figs 7, 8). Most of the calcified plaques are presented as smooth protruding sign on VIE as shown in Figures 7-10. However, the presence of extensively calcified plaques along the coronary artery could result in irregular intraluminal changes in the coronary wall. Figure 11 is an example of VIE visualization of a patient with extensively calcified plaque at the LAD with irregular intraluminal appearances in the coronary wall.

Mixed plaques

Irregular intraluminal appearances are commonly seen in mixed plaques on VIE because different components are contained within the plaques. This indicates that the coronary wall undergoes different stages of remodelling process, which consists of both stable stage involving formation of calcified plaques and unstable period involving deposition of non-calcified plaques which contain lipid-rich components. Figure 12 is an example of mixed plaques at the proximal segment of LAD with non-calcified component representing the majority of the content, with corresponding VIE showing irregular intraluminal changes in the coronary wall caused by the mixed plaques. Figure 13 is another example of mixed plaques at the proximal segment of LAD with calcified component representing the majority of the content, and the corresponding VIE demonstrates irregular intraluminal changes.

VIE visualization of coronary stents

VIE visualization has been reported to serve as a potential tool for follow-up of endovascular stent grafting and stenting as it allows demonstration of the intraluminal views of the artery wall and stent surface [22, 23, 26-29].

Normal stent appearances

Since CT attenuation of coronary stents is much higher than that of contrast-enhanced blood, stents are easily visualized on VIE as high density structure with uniform appearance inside the coronary arteries, depending on the location where the stents are deployed. Figure 14 shows a patent coronary stent placed in the right coronary artery with smooth circular appearance on VIE visualization. Furthermore, VIE visualization also assists detection of stent position in relation to the coronary ostia

through providing 3D intraluminal views. Figure 15 is an example of left coronary stent which is placed at the proximal segment of LAD, with patency of the coronary ostia arising from the LAD.

In-stent restenosis appearances

In-stent restenosis appears as low-attenuation area within the high-density metallic stents on 2D CT images. On VIE visualization, the in-stent restenosis is demonstrated as irregular appearances on the coronary wall with subsequent coronary lumen stenosis. Figure 16 shows VIE visualization of in-stent restenosis in the LAD with irregular coronary wall change, while Figure 17 is another example with significant in-stent restenosis in the LAD with corresponding irregular coronary wall changes and lumen stenosis as visualized on VIE.

Summary and conclusion

In this pictorial essay, we have demonstrated a spectrum of VIE findings of coronary plaques and coronary stents inclusive of both normal lumen appearances and pathological changes caused by plaques or stents. Although VIE is not recommended as a routine tool for detection of coronary plaques or stents, it can be used as a complimentary approach to conventional visualizations for accurate assessment of coronary plaques and stents.

3D VIE visualization shows potential applications for assessment of coronary plaques in terms of plaque characterization and intraluminal appearances, while in coronary stenting, VIE can demonstrate the intraluminal coronary stents in relation to coronary ostia or detect luminal changes due to in-stent restenosis. VIE visualization is considered valuable for enhancing our understanding of the effect of coronary plaques and stents on coronary wall and subsequent clinical outcomes [21, 25, 30]. VIE

visualization tool presented in this review could contribute to overcome some of the image processing limitations for quantitative assessment of atherosclerotic plaques [31]. The main advantages of VIE visualization are summarised in the table, although further studies are needed to verify the VIE findings and associated clinical value.

Acknowledgements

This work has been supported by research grant from Natural Science Foundation of China (grant 81271542), grant for Excellent Talents from Beijing city (2011D003034000030), and grant for High Levels of Health Technical Personnel in Beijing City Health System (2013-3-011).

References

[1] Schuijf JD, Pundziute G, Jukema JW, et al. Diagnostic accuracy of 64-slice multislice computed tomography in the non-invasive evaluation of significant coronary artery disease. Am J Cardiol 2006; 98: 145-148

[2] Vanhoenacker P, Heijenbrok-Kal M, Van Heste R, et al. Diagnostic performance of multidetector CT angiography for assessment of coronary artery disease: meta-analysis. Radiology 2007; 244: 419-428

[3] Sun Z, Lin C, Davidson R, Dong C, Liao Y. Diagnostic value of 64-slice CT angiography in coronary artery disease: A systematic review. Eur J Radiol 2008; 67: 78-84

[4] Abdulla J, Abildstrom Z, Gotzsche O, Christensen E, Kober L, Torp-Pedersen C. 64-multislice detector computed tomography coronary angiography as potential alternative to conventional coronary angiography: a systematic review and meta-analysis. Eur Heart J 2007; 28: 3042-3050

[5] Sun Z, Cao Y, Li HF. Multislice computed tomography angiography in the diagnosis of coronary artery disease. J Geriatr Cardiol 2011; 8: 104-113

[6] Sun Z, Jiang W. Diagnostic value of multislice CT angiography in coronary artery disease: A meta-analysis. Eur J Radiol 2006; 60: 279-286

[7] Xu L, Zhang Z. Coronary CT angiography with low radiation dose. Int J Cardiovasc Imaging 2010; Suppl 1: 17-25

[8] Yang L, Zhou T, Zhang R, et al. Meta-analysis: diagnostic accuracy of coronary CT angiography with prospective ECG gating based on step-and-shoot, Flash, and volume modes for

detection of coronary artery disease. Eur Radiol 2014; May 28 (Epub ahead of print) DOI 10.1007/s00330-014-3221-y

[9] Sun Z, Ng KH. Diagnostic value of coronary CT angiography with prospective ECG-gating in the diagnosis of coronary artery disease: a systematic review and meta-analysis. Int J Cardiovasc Imaging 2012; 28: 2109-2119

[10] von Ballmoos MW, Haring B, Juillert P, Alkadhi H. Meta-analysis: diagnostic performance of low-radiation-dose coronary computed tomography angiography. Ann Intern Med 2011; 154: 413-420

[11] Rodriguez-Granillo GA, Rosales MA, Degrossi E, Durbano I, Rodriguez AE. Multislice CT coronary angiography for the detection of burden, morphology and distribution of atherosclerotic plaques in the left main bifurcation. Int J Cardiovasc Imaging 2007; 23: 389–392

[12] Schmid M, Pflederer T, Jang IK, et al. Relationship between degree of remodelling and CT attenuation of plaque in coronary atherosclerotic lesions: an in-vivo analysis by multi-detector computed tomography. Atherosclerosis 2008; 197: 457-464

[13] Motoyama S, Kondo T, Sarai M, et al. Multislice computed tomographic characteristics of coronary lesions in acute coronary syndromes. J Am Coll Cardiol 2007; 50:319–26

[14] Schuijf JD, Beck T, Burgstahler C, et al. Differences in plaque composition and distribution in stable coronary artery disease versus acute coronary syndromes; non-invasive evaluation with multi-slice computed tomography. Acute Cardiac Care 2007; 9: 48–53

[15] Motoyama S, Sarai M, Harigaya H, et al. Computed tomographic angiography characteristics of atherosclerotic plaques subsequently resulting in acute coronary syndrome. J Am Coll Cardiol 2009; 54: 49-57

[16] Burke AP, Kolodgie FD, Farb A, Weber D, Virmani R. Morphological predictors of arterial remodelling in coronary atherosclerosis. Circulation 2012; 105: 297-303

[17] Ehara S, Kobayashi Y, Yoshiyama M, et al. Spotty calcification typifies the culprit plaque in patients with acute myocardial infarction: an intravascular ultrasound study. Circulation 2004; 110: 3424–3429

[18] Maurovich-Horvat P, Hoffmann U, Vorpahl M, Nakano M, Virmani R, Alkadhi H. The napkin-ring sign: CT signature of high-risk coronary plaques? JACC Cardiovasc Imaging 2010; 3 (4): 440–444

[19] Sharif F, Murphy RT. Current status of vulnerable plaque detection. Catheter Cardiovasc Interv 2010; 75: 135–144

[20] Sun Z, Zheng H. Effect of suprarenal stent grafts on the renal artery with ostial calcification observed on CT virtual intravascular endoscopy. Eur J Vasc Endovasc Surg 2004; 28: 534-542

[21] Sun Z, Dimpudus FJ, Nugroho J, Adipranoto JD. CT virtual intravascular endoscopy assessment of coronary artery plaques: A preliminary study. Eur J Radiol 2010; 75: e112-e119

[22] Sun Z. multislice CT angiography in post-aortic stent grafting: A pictorial essay. Korean J Radiol 2006; 7: 205-211

[23] Sun Z, Allen YB, Nadkarni S, Knight R, Hartley DE, Lawrence-Brown MM. CT virtual intravascular endoscopy in the visualization of fenestrated stent-grafts. J Endovasc Ther 2008; 15: 42-51

[24] Sun Z, Al Dosari S, Ng C, al-Mumntshari A, Almaliky S. Multislice CT virtual intravascular endoscopy of pulmonary embolism: A pictorial review. Korean J Radiol 2010; 11: 222-230

[25] Sun Z, Cao Y. Multislice CT angiography assessment of left coronary artery: correlation between bifurcation angle and dimensions and development of coronary artery disease. Eur J Radiol 2011; 79: e90-e95

[26] Sun Z, Winder RJ, Kelly BE, Ellis PK, Kennedy PT, Hirst DG. Diagnostic value of CT virtual intravascular endoscopy in aortic stent grafting. J Endovasc Ther 2004; 11(1): 13-25

[27] Sun Z, Winder RJ, Kelly BE, Ellis PK, Hirst DG. CT virtual intravascular endoscopy of abdominal aortic aneurysms treated with suprarenal endovascular stent grafting. Abdom Imaging 2003; 28: 580-587

[28] Sun Z, Gallagher E. Multislice CT virtual intravascular endoscopy for abdominal aortic aneurysm stent grafts. J Vasc Interv Radiol 2004; 15: 961-970

[29] Almutairi A, Sun Z, Ng C, Al-Safran ZA, Al-Mulla AA, Al-Jamaan AI. Optimal scanning protocols of 64-slice CT angiography in coronary artery stents: An in vitro phantom study. Eur J Radiol 2010; 74(1): 156-160

[30] Sun Z. Coronary CT angiography in coronary artery disease: correlation between virtual intravascular endoscopic appearances and left bifurcation angulation and coronary plaques. Biomed Res Int 2013; 2013: 732059

[31] Jodas DS, Pereira AS, Tavares JRMS. A review of computational method applied for identification and quantification of atherosclerotic plaques in images. Expert Sys Appl 2016;46:1-14

Figure legends

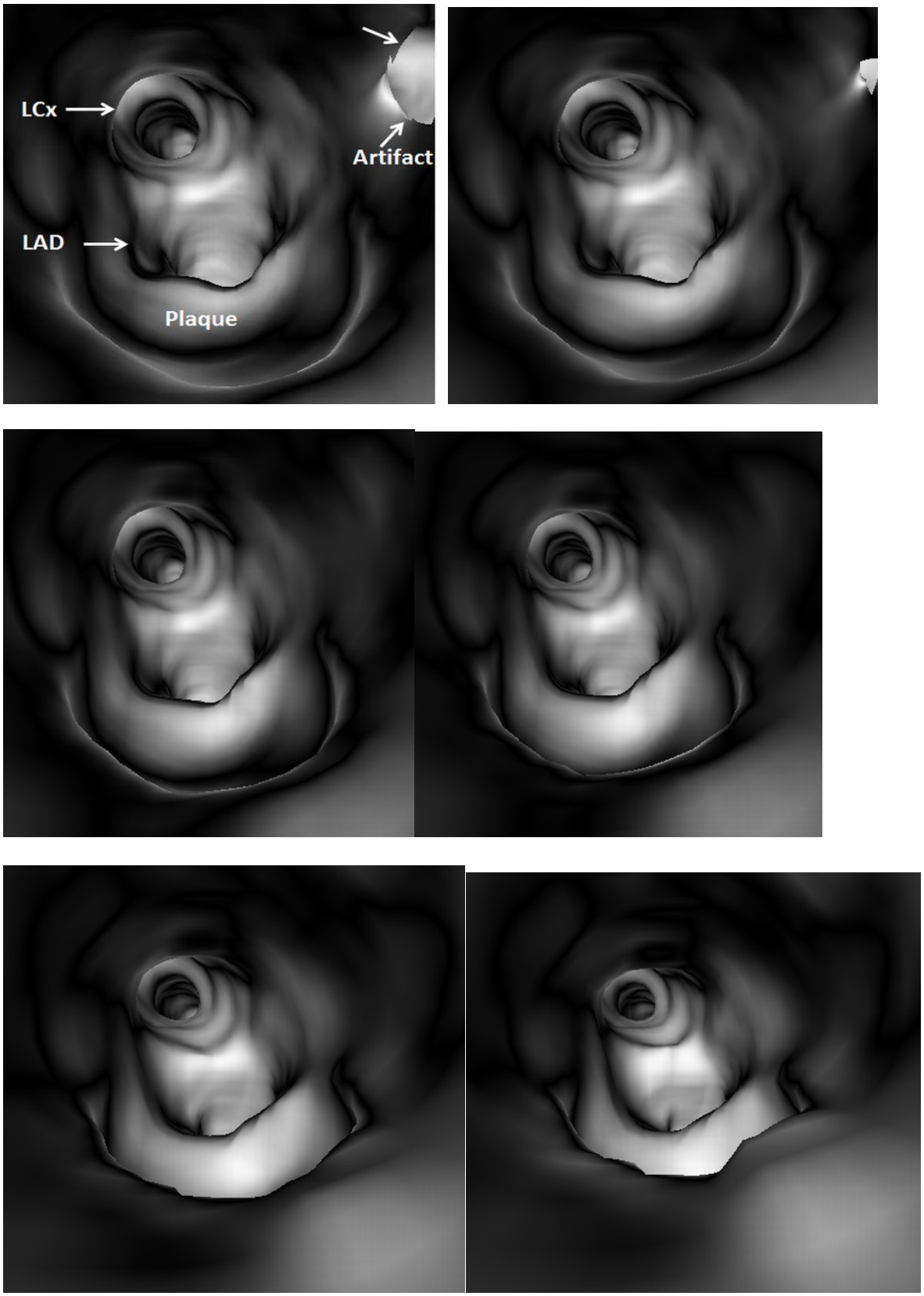

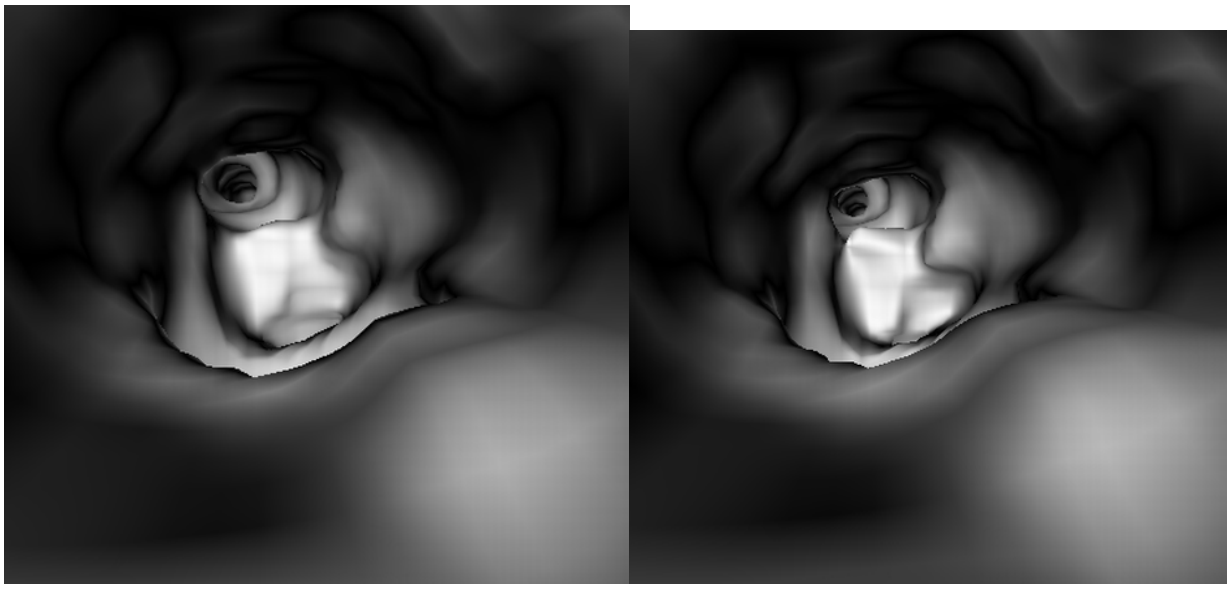

Figure 1. VIE visualization of coronary wall and plaque depends on appropriate selection of CT threshold. Figures A to H are a series of VIE images viewing the LAD and LCx ostia a well as coronary plaque arising from the LAD with selection of CT threshold of 160 HU, 180 HU, 200 HU, 220 HU, 240 HU, 260 HU, 280 HU, 300 HU, respectively. As shown in the images, when upper CT threshold is lower than 200 HU, artifact (arrow) appears in the coronary wall. When upper CT threshold is higher than 240 HU, visualization of coronary plaque and coronary ostia is affected. Thus, the appropriate CT threshold for visualization of coronary ostia and plaque is between 200 and 220 HU.

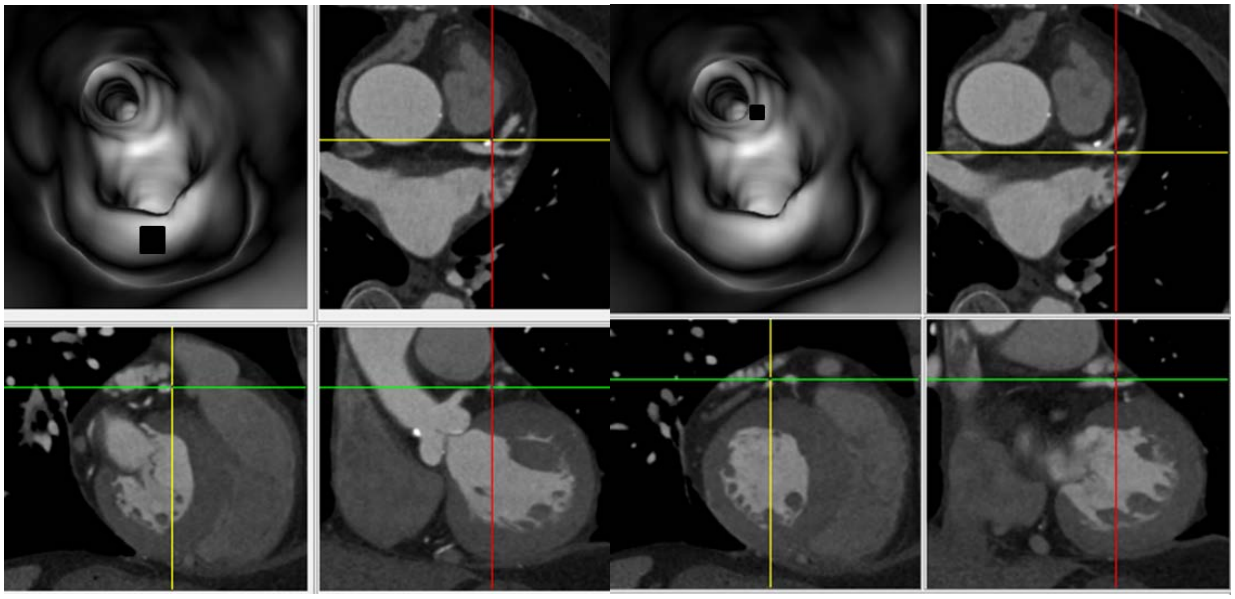

Figure 2. Correlation of VIE visualization of coronary anatomy and plaque with orthogonal views. A. The viewing position is placed at the coronary plaque in the LAD ostium, and confirmation of the ostium is determined by checking the axial, coronal and sagittal views. B. The viewing position is focused on the LCx ostium which is confirmed by checking these orthogonal view

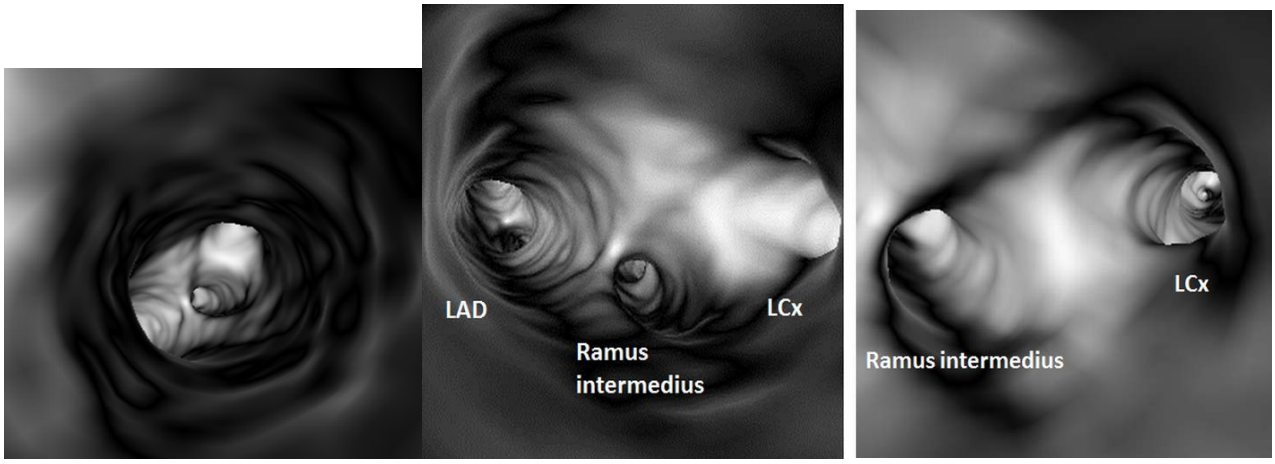

Figure 3. VIE visualization of normal left coronary ostia. A. VIE view of the left main coronary artery. B and C. VIE demonstrates the left coronary ostia with regard to their intraluminal relationship.

Figure 4. VIE visualization of normal right coronary ostium with regular smooth appearance.

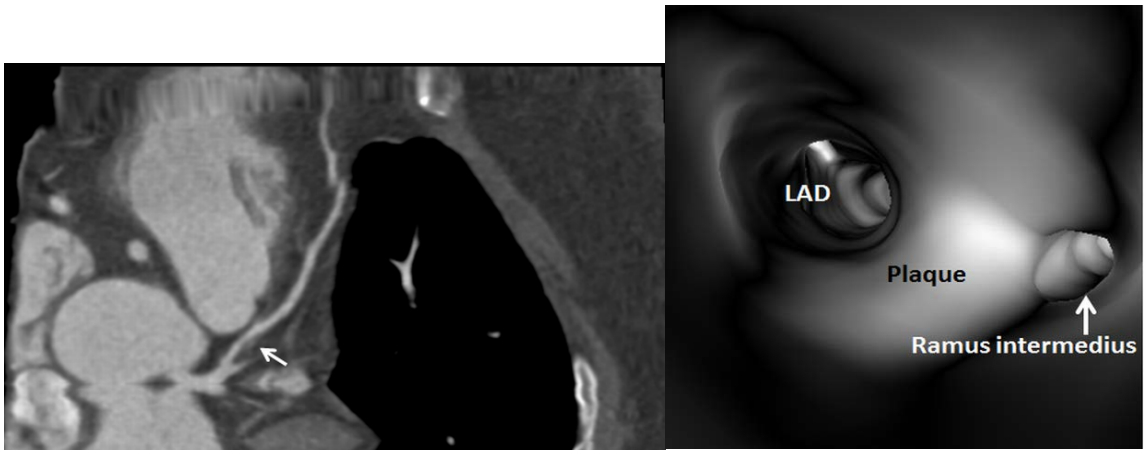

Figure 5. VIE visualization of non-calcified plaque. A. Curved planar reformatted image shows non-calcified plaque (arrow) at the proximal segment of LAD in a 71-year-old man. B. Corresponding VIE shows the plaque arising from the inferior wall of LAD with smooth appearance, with involvement of the ramus intermedius ostium (arrow).

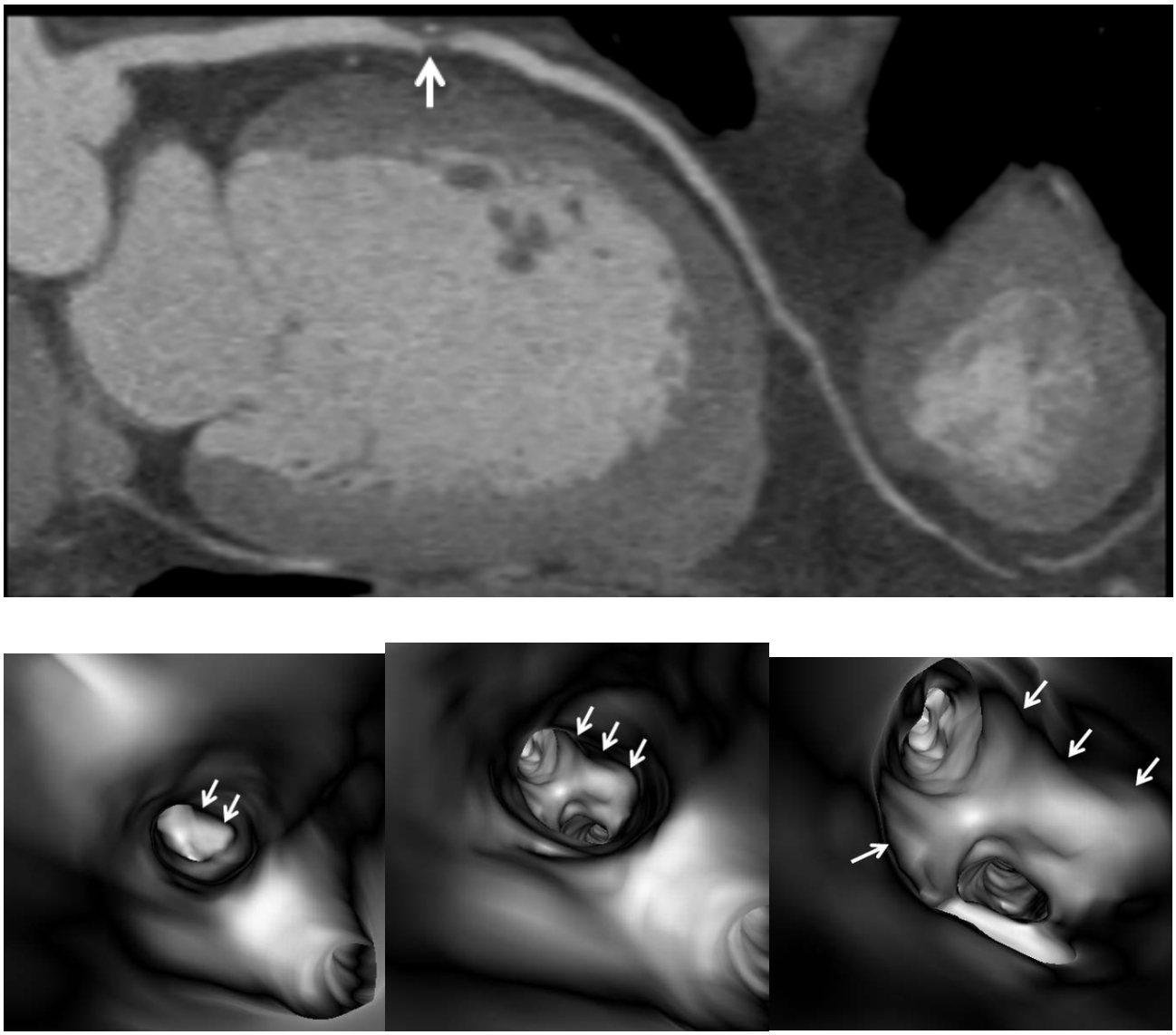

Figure 6. VIE visualization of non-calcified plaque with changing CT threshold for clear demonstration of coronary wall and plaque appearances. A. Curved planar reformatted image shows non-calcified plaque (arrow) at the proximal segment of LAD in a 59-year old male. B. Both coronary plaque and LAD ostium (arrows) could not be clearly assessed when the upper CT threshold is selected at 130 HU. C. When the upper CT threshold is reduced from 130 HU to 60 HU, the plaque (arrows) and LAD ostia are clearly visualized on VIE. D. VIE close view (arrows) indicates the relationship between plaque and the LAD ostium with upper CT threshold set at 60 HU.

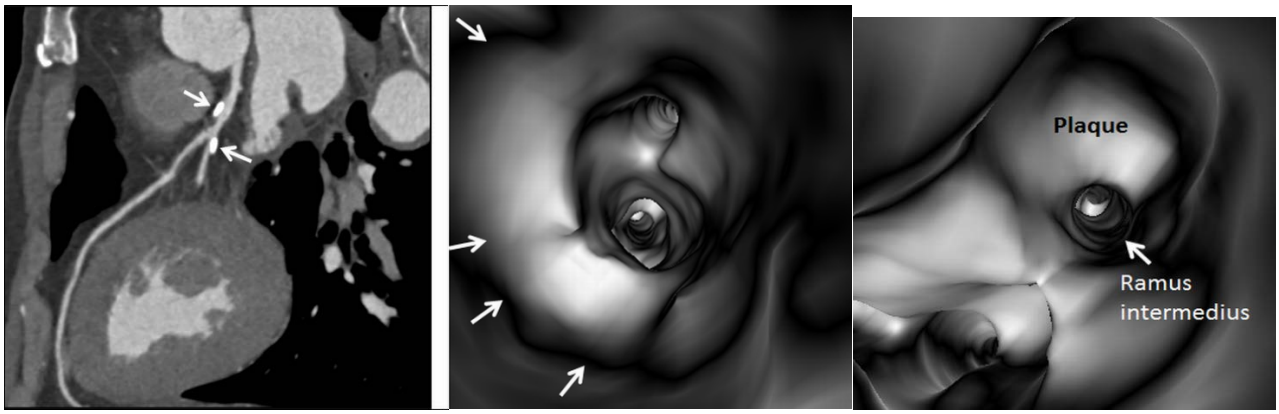

Figure 7. VIE visualization of eccentric calcified plaques. A. Curved planar reformatted image reveals calcified plaques at the left main stem and LAD coronary arteries in an 80-year-old male. B. VIE shows the calcified plaque (arrows) arising from the superior wall of LAD with involvement of LAD ostium. C. VIE close view shows that the plaque surrounds the ramus intermedium ostium (arrow).

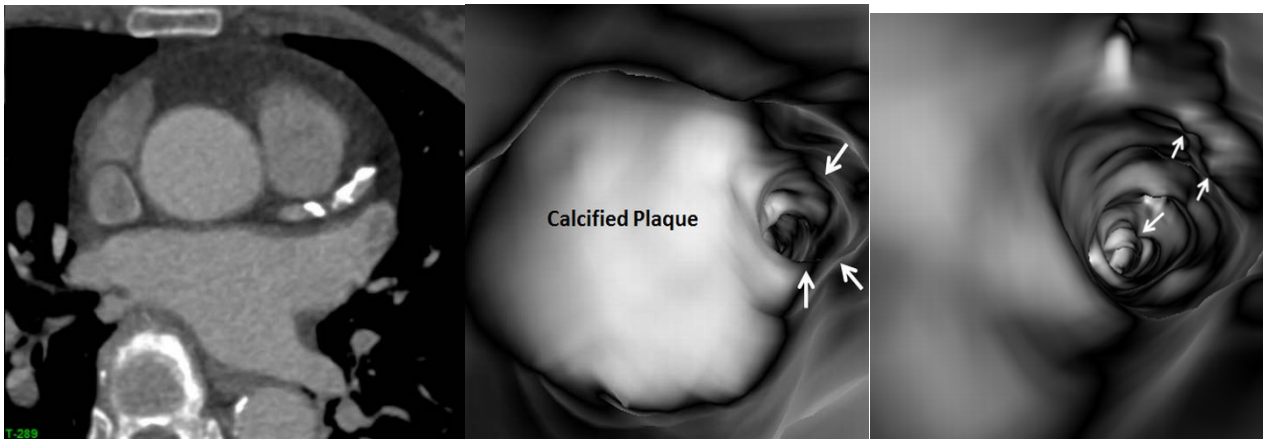

Figure 8. VIE visualization of eccentric calcified plaques. A. 2D axial image shows calcified plaques mainly locating in the superior wall of LAD in a 73-year-old female. B. VIE demonstrates a huge intraluminal plaque occupying the LAD ostium (arrows). C. VIE view of distal LAD reveals irregular coronary wall (arrows) caused by the extensively calcified plaque.

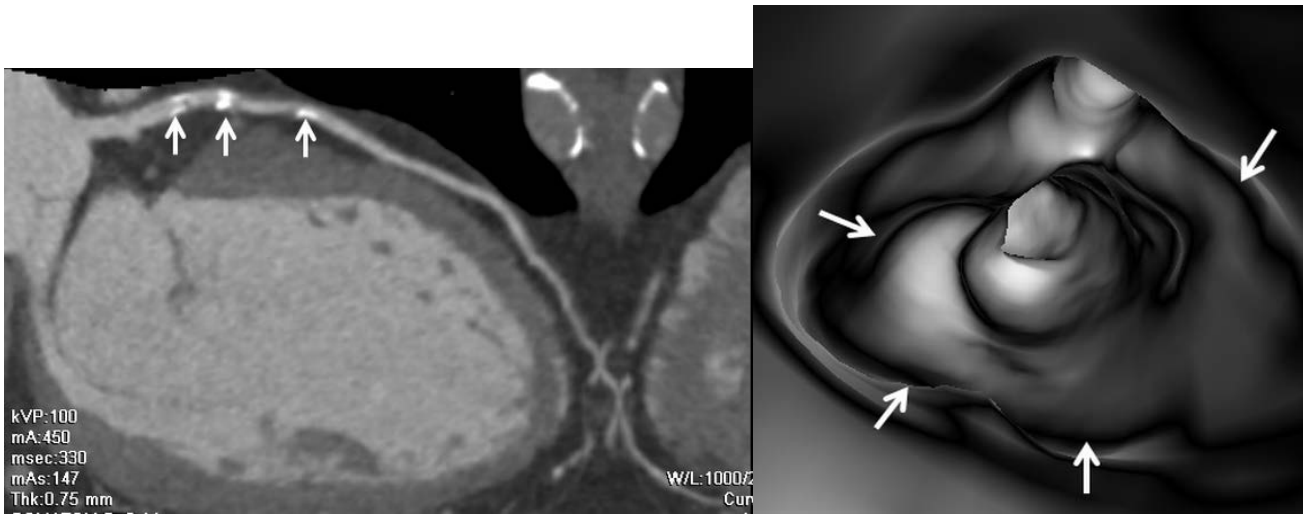

Figure 9. VIE visualization of concentric calcified plaques. A. Curved planar reformatted image shows calcified plaques at the proximal segment of LAD in a 61-year-old man. B. VIE confirms that the concentrically calcified plaques (arrows) surround the LAD osium.

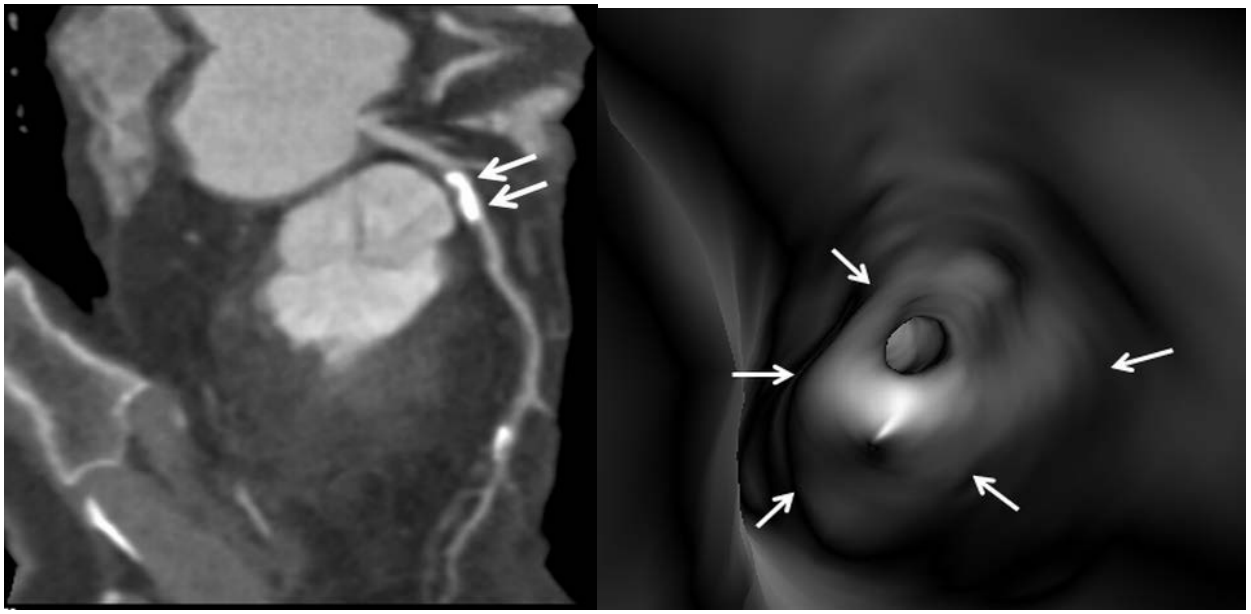

Figure 10. VIE visualization of concentric calcified plaque. A. Curved planar reformatted image shows highly calcified plaque at the proximal segment of LAD in a 49-year-old woman. B. VIE shows

significant stenosis of LAD caused by the calcified plaque (arrow). C. VIE close view of the concentrically calcified plaque covering the LAD ostium.

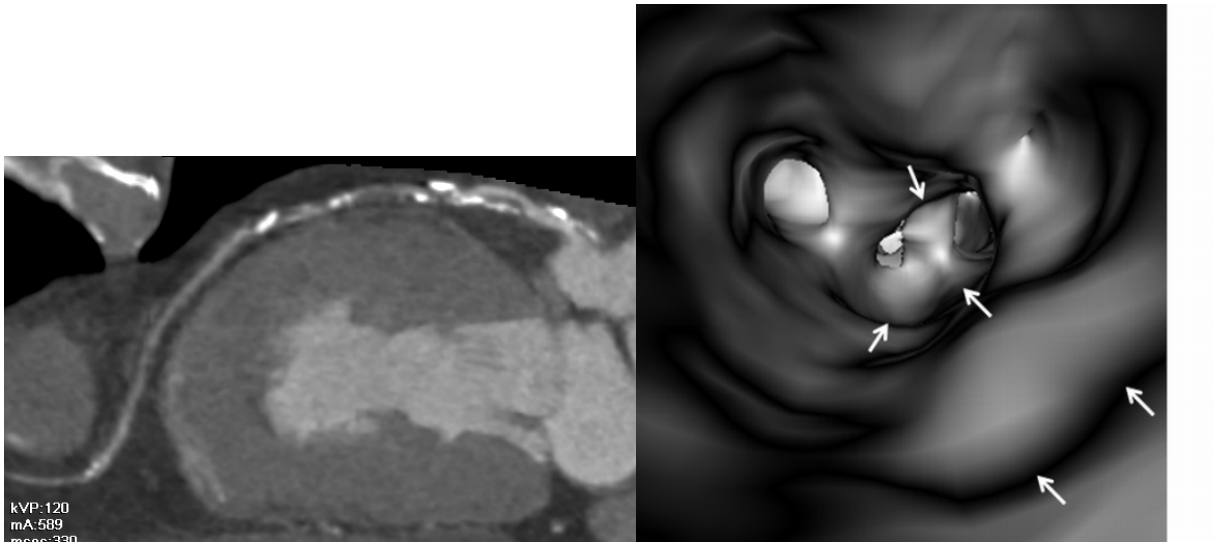

Figure 11. VIE visualization of extensively calcified plaques. A. Curved planar reformatted image shows extensively calcified plaques in the LAD with some low-attenuation areas representing non-calcified component in a 58-year-old male. B. Corresponding VIE demonstrates irregular coronary lumen changes (arrows) caused by the extensively calcified plaques.

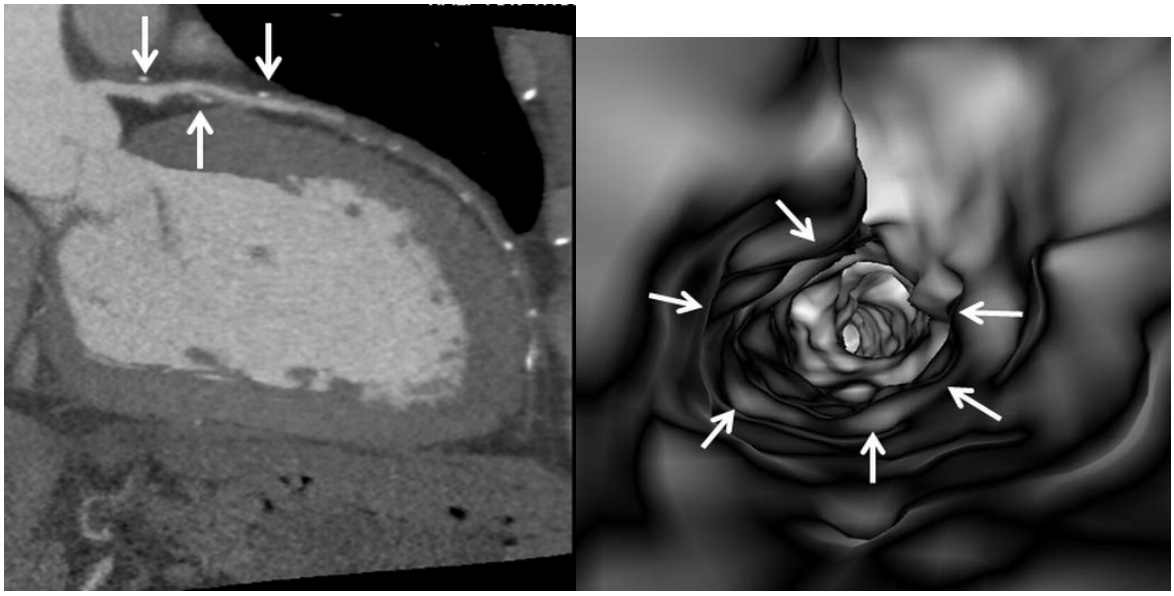

Figure 12. VIE visualization of mixed plaques. A. Curved planar reformatted image shows mixed plaques with spotty calcification at the proximal segment of LAD in a 68-year-old male. B. VIE indicates irregular coronary wall changes (arrows) due to different components within the plaques.

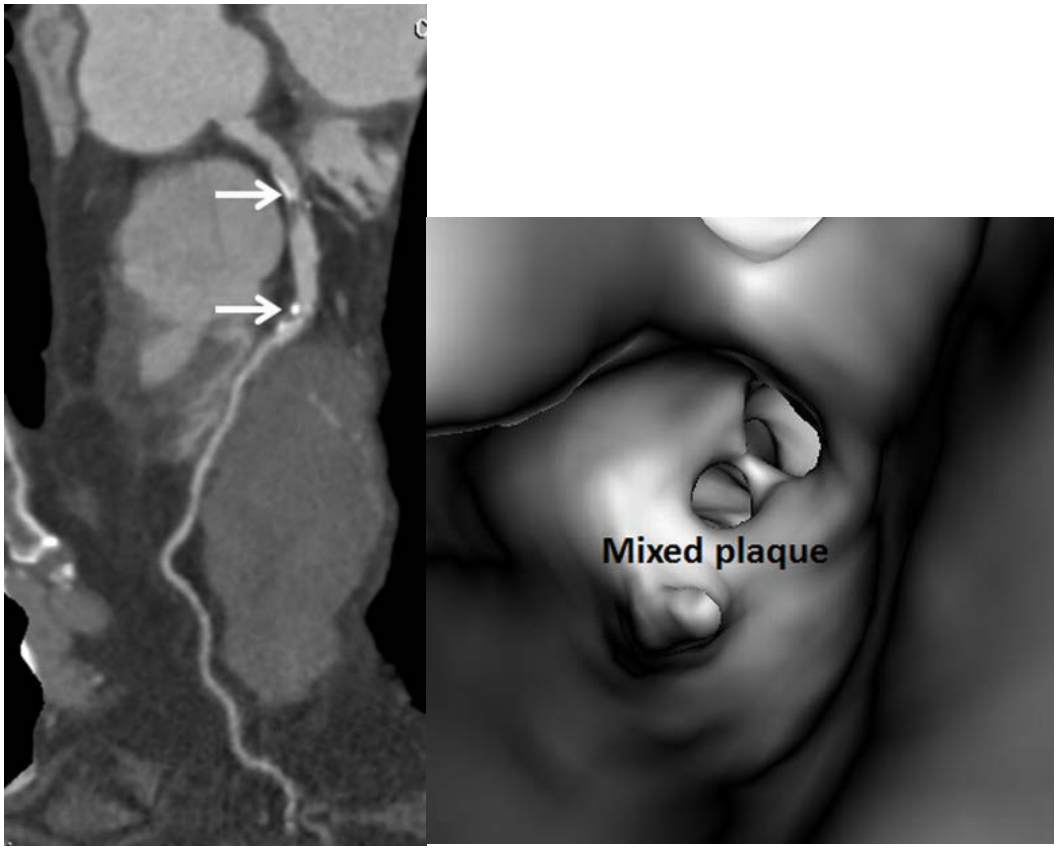

Figure 13. VIE visualization of mixed plaques. A. Curved planar reformatted image shows mixed plaques with calcified components clearly present within the plaques in a 55-year-old male. B. VIE demonstrates irregular coronary wall due to presence of mixed plaques.

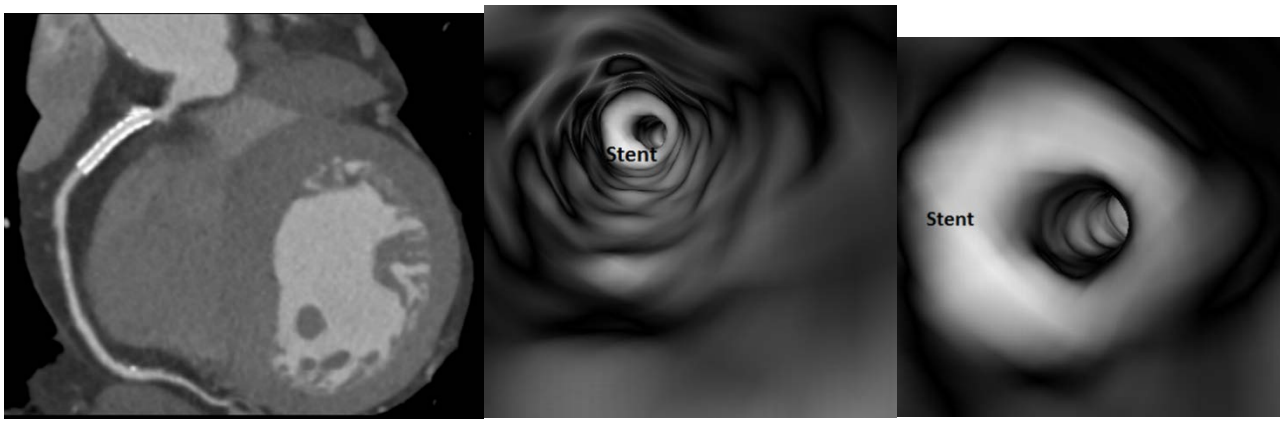

Figure 14. VIE visualization of patent coronary stents. A. Curved planar reformatted image shows a patent coronary stent in the RCA in a 69-year-old male. B. VIE visualization of the coronary stent when the view is positioned at the proximal segment of RCA. C. Close VIE visualization of stent surface shows smooth circular appearance inside the RCA.

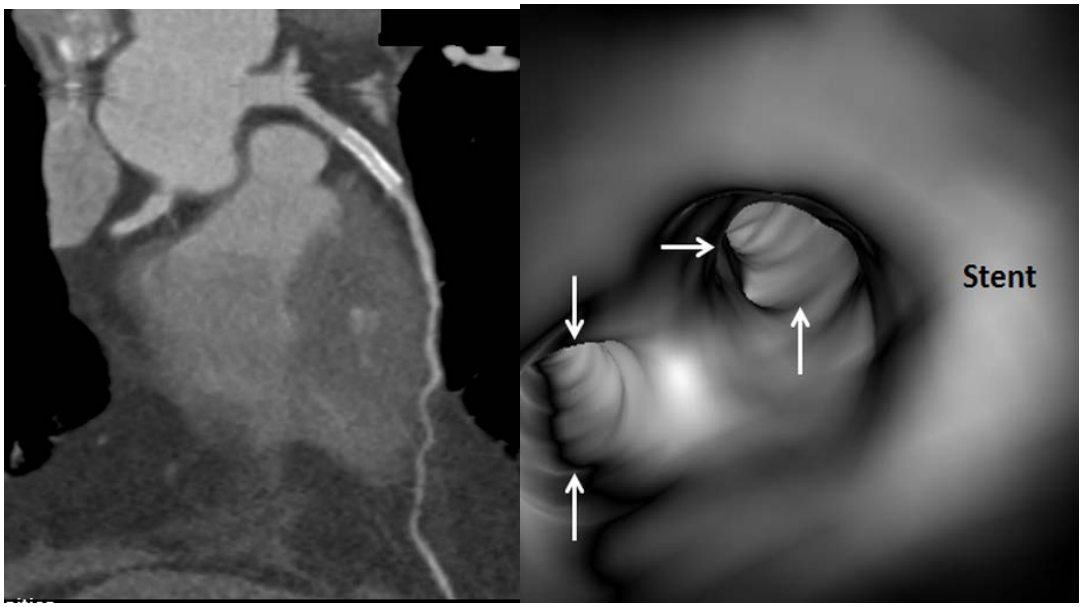

Figure 15. VIE visualization of coronary stent in relation to the coronary ostia. A. Curved planar reformatted image shows a patent coronary stent in the LAD in a 47-year-old man. B. VIE indicates the circular smooth appearance of coronary stent relative to the LAD ostium (arrows).

Figure 16. VIE visualization of coronary in-stent restenosis. A. Curved planar reformatted image shows low-attenuation area (arrows) with suspected in-stent restenosis in the LAD stent in a 65-year-old man. B and C. Distal and proximal VIE views of the LAD lumen confirm the irregular wall changes (arrows) due to in-stent restenosis.

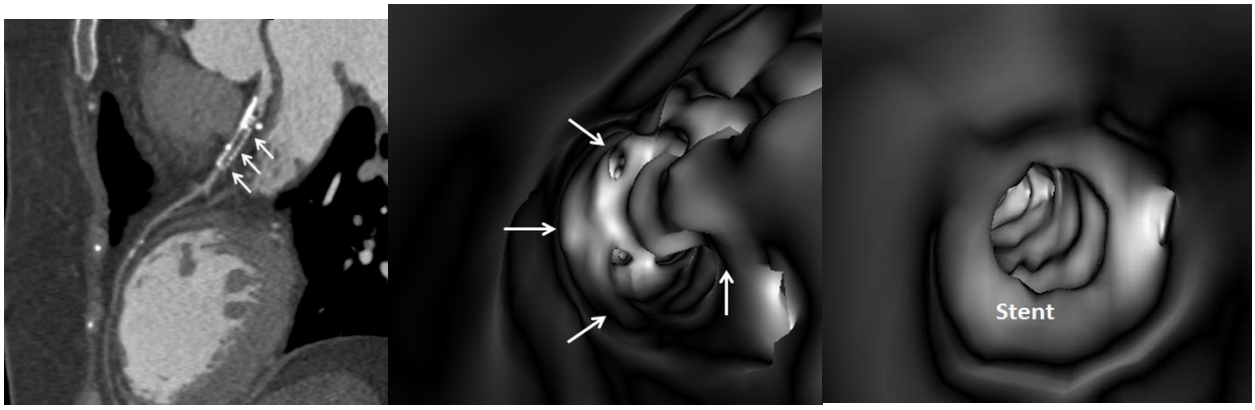

Figure 17. VIE visualization of coronary in-stent restenosis. A. Curved planar reformatted image demonstrates low-attenuation area (arrows) in the LAD stent in a 50-year-old woman. B. VIE confirms

significant lumen stenosis with irregular wall changes (arrows). C. The coronary stent in the LCx remains patent on VIE visualization.